

Wideband and Ultra-Wideband Characterization of Three-Dimensional MIMO Wireless Channels

A. M. Pistea and H. Saligheh Rad

Abstract—In this paper, we compute cross-correlation functions (CCF)s between space-time-frequency (STF) transfer functions of two sub-channels of three-dimensional (3D) outdoor wideband (WB) and ultra-wideband (UWB) multiple-input multiple-output (MIMO) wireless channels. Such a 3D channel modeling is demanding to consider both azimuthal and elevation multipath propagation waveforms. Using the derived CCF and for a multiple-input single-output system (MISO), we calculate coherence bandwidth (CB) and power spectral density (PSD) at mobile station (MS), and in a stationary scenario. Numerical analysis shows that both CB and PSD highly depend the channel bandwidth, while PSD is also influenced by the elevation distribution of multipath waveforms.

Index Terms—Wideband, ultra-wideband, MIMO, 3D non-isotropic propagation.

I. INTRODUCTION

COMBINATION of the emerging multiple-input multiple-output (MIMO) technology with wideband (WB) and ultra-wideband (UWB) communication brings the necessity for wireless channel models to be more sophisticated by taking into account more complex propagation phenomena [1]. On top of that, it is not clear if conventional WB models can be reliably used to characterize UWB propagation. One method to create WB and UWB channel models is to derive them as an extension of existing narrowband (NB) models. In this paper, we extend the three-dimensional (3D) NB propagation model described in [2] to comprehensively analysis WB and UWB channels. The model statistically describes outdoor WB and UWB MIMO wireless channels based on 3D space-time-frequency (STF) channel transfer functions (CTFs). Using the 3D CTFs, we determine the STF cross-correlation function (CCF) between two sub-channels of a mobile multicarrier MIMO channel. We use the CCF to analyze the coherence bandwidth (CB) for both WB and UWB channels. Fourier analysis of the CCF is used to determine power spectral density (PSD) of the two types of WB and UWB channels. The rest of this paper is organized as follows: in Section 2, the 3D channel model is described and the CCF expression is derived. In Section 3, the CCF is numerically evaluated, including Fourier analysis of the CCF and the relationship between CCF and CB. Conclusions are summarized in Section 4.

Manuscript received September 16, 2011. The associate editor coordinating the review of this letter and approving it for publication was A. Panagopoulos.

A. M. Pistea is with the Military Technical Academy, Bucharest, Romania (e-mail: ampistea@gmail.com).

H. S. Rad is with the Laboratory for Advanced MR Imaging and Spectroscopy (LAMIS), Medical Physics Department, Tehran University of Medical Sciences (TUMS), Tehran, Iran, and with the Research Center for Science and Technology in Medicine (RCSTIM), Imam Hospital, Tehran, Iran.

Digital Object Identifier 10.1109/LCOMM.2011.112311.111948

II. THREE DIMENSIONAL MODEL DESCRIPTION

In this section, we identify existing differences between NB against WB/UWB channel modeling. We also present employed notations and assumptions for WB/UWB MIMO channels, and in a 3D non-isotropic random scattering medium.

a) NB and WB/UWB Wireless Propagation Channels:

There are two major differences between NB versus WB/UWB channels: i) variations of most channel parameters with frequency and ii) tendency to group multipath waveforms into clusters [3]. Taking into consideration these two major changes, we propose necessary parameters to be included in WB/UWB MIMO propagation modeling as follows: 1) frequency selectivity term, $(\frac{\omega_{bw}}{\omega})^\eta$, where ω is the channel central frequency, ω_{bw} is the channel bandwidth and η is the path-loss exponent [4], 2) the l th cluster delay - T_l , and the i th path delay of the l th cluster - τ_{il} , 3) frequency selective multipath gain, $g_{mp,il} = \frac{1}{2\omega\tau_{il}}$ and 4) specific antenna propagation patterns (APP). For the NB channel, it is assumed that the response of the antenna does not significantly change over the frequency range of interest. The same assumption fairly holds for WB channels since their relative bandwidth is still a small fraction of the central frequency [1]. However in UWB channels, APP is a function of frequency which introduces the main difference between WB and UWB channel models. Therefore, depending on the signal bandwidth in WB/UWB channel modeling, we have two approaches to compute APPs: a) for WB channels, APP is calculated depending on the central frequency and b) for UWB channels, APP is integrated as an average across all frequencies of the transmitted signal.

b) *Channel Modeling Scenario*: Throughout this paper superscripts B and M indicate variables at the base station (BS) and at the mobile station (MS) sides, respectively. The proposed channel model is established based on the following scenario:

BS and MS: We assume BS antenna array is fixed in the coordinate, O^B . MS antenna array moves with its coordinate, O^M , and with a constant speed, $V(\frac{m}{sec})$. The complex APPs of the p^{th} antenna at the BS and the m^{th} antenna at the MS, are represented by $G_p^B(\Theta^B; \Omega^B; \omega)$ and $G_m^M(\Theta^M; \Omega^M; \omega)$. These pattern functions reflect the influence of the direction of departure (DOD) azimuthal angle of BS (Θ_{il}^B) and direction of arrival (DOA) azimuthal angle of MS, (Θ_{il}^M). Also show the effect of the DOD elevation angle of BS (Ω_{il}^B) and DOA elevation angle of MS, (Ω_{il}^M). These expressions give the response of antennas in terms of the azimuth and the elevation propagation directions, the central frequency (WB channels) or frequency band (UWB channels). As these functions are periodic in terms of Θ and Ω we represent them by their Fourier series coefficients (FSCs) [2], [4]. Table I presents

TABLE I: 3D WB and UWB Antenna Propagation Patterns

APP	Rectangular antenna, $G(\Theta; \Omega; \omega), \forall \Theta \in [-\pi, \pi], \forall \Omega \in [-\pi, \pi]$
WB	$G_0 \sin \Omega \frac{\sin(\frac{\omega}{2c} h \sin \Theta \cos \Omega)}{\frac{\omega}{2c} h \sin \Theta \cos \Omega} \frac{\sin(\frac{\omega}{2c} h \sin \Theta \sin \Omega)}{\frac{\omega}{2c} h \sin \Theta \sin \Omega} d\omega$
UWB	$\frac{\int_{f_L}^{f_H} j G_0 \sin \Omega \frac{\sin(\frac{\omega}{2c} h \sin \Theta \cos \Omega)}{\frac{\omega}{2c} h \sin \Theta \cos \Omega} \frac{\sin(\frac{\omega}{2c} h \sin \Theta \sin \Omega)}{\frac{\omega}{2c} h \sin \Theta \sin \Omega} d\omega}{(f_H - f_L)}$

the APPs of an omnidirectional antenna used for WB/UWB communications [7].

Environment: Non-isotropic propagation environment around BS and MS is described by probability density function (pdf) of the azimuth angle spread (AAS), $f_A(\Theta)$ [4] as well as the pdf of the EAS, $f_E(\Omega)$ [2]. In order to satisfy the requirements of a pdf for realistic EAS, we assume as $f_E(\Omega) = 0$ for $|\Omega| \leq \frac{\pi}{2}$. For $|\Omega| > \frac{\pi}{2}$, it is defined using the following distributions [2]:

$$\begin{aligned} \text{EAS I: } f_E(\Omega) &= \frac{\Gamma(a+1) \cos^{2a}(\Omega)}{\sqrt{\pi} \Gamma(a+\frac{1}{2})} \\ \text{EAS II: } f_E(\Omega) &= \frac{2|\sin(\Omega)|^{2a} \cos(\Omega)}{2a+1} \end{aligned} \quad (1)$$

where $\Gamma(u)$ is the gamma function and $a \geq 0$ indicates the degree of urbanization. Parameter a depends on the number of waves scattered into the third dimension of space. Using different values for a , the model describes different urban environments. For example, by increasing the value of the parameter a , the model covers rural to urban propagation media, where necessary FSCs in order to accurately describe the EAS increases.

Based on the type of the propagation environment, NB or WB/UWB, and characteristics of the BS or MS, we determine the expression for a new CTF, $h_{pm}(t, \omega)$. This CTF corresponds to each WB/UWB MIMO sub-channel, consisting of the transmitting antenna element located at a_p^B , the propagation environment and the receiving antenna element located at a_m^M :

$$h_{pm}(t, \omega) = \sum_{l=1}^L \sum_{i=1}^I G_p^B(\Theta_{il}^B, \Omega_{il}^B; \omega) G_m^M(\Theta_{il}^M, \Omega_{il}^M; \omega) \times g_{mp,il} e^{j(\phi_{il} + \frac{\omega}{c} V^T \Psi_{il}^M - \omega T_{pm,l} - \omega \tau_{pm,il}(t))} \left(\frac{\omega_{bw}}{\omega}\right)^\eta \quad (2)$$

The CTF presented in (2) is the result of the summation of $L * I$ dominant paths in L dominant clusters, each including I dominant paths. Each i^{th} received waveform (within l^{th} cluster) is associated with a path attenuation gain, $g_{mp,il}$, a path phase shift, ϕ_{il} , a path time-varying delay, $\tau_{pm,il}$ (due to the mobility of MS), a cluster delay, $T_{pm,l}$ and a complex gain determined by the BS and the MS antenna patterns. [7]. The term $\frac{\omega}{c} V^T \Psi_{il}^M$ represents the Doppler shift of the i^{th} received wave within the l^{th} cluster. The parameter c is the light speed and $\Psi_{il}^M \triangleq [\cos(\Omega) \cos(\Theta) \cos(\Omega) \sin(\Theta) \sin(\Omega)]^T$ is the 3D unity vector pointing to the DOA of the i^{th} path to the MS and $[\cdot]^T$ is the transpose operator. The CCF between the TFs of two arbitrary sub-channels of a MIMO channel, $h_{pm}(t_1, \omega_1)$ and $h_{qn}(t_2, \omega_2)$, is defined as: $R_{pm,qn}(t_1, t_2, \omega_1, \omega_2) \triangleq E[h_{pm}(t_1, \omega_1) h_{qn}^*(t_2, \omega_2)]$, where $E[\cdot]$ is the expectation operator. Using equation (2), the definition of the MS, the scattering environment and the BS, and based on the results presented in [4], we obtain an expression for the CCF as follows:

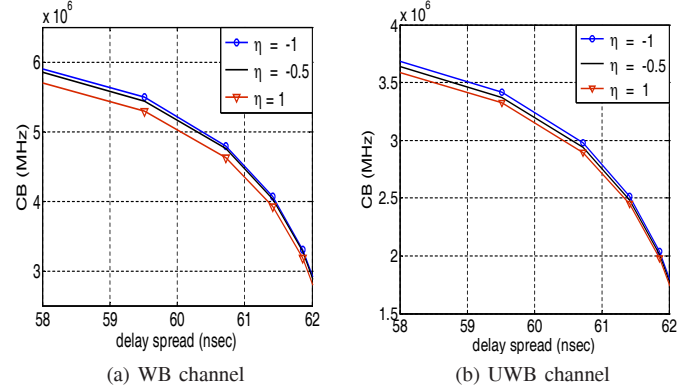


Fig. 1: Coherence bandwidth, depending on the delay spread, σ , $t_1 = t_2 = 1sec$, $V=10$ mps, MISO communication system, with different pathloss exponents.

$$R_{pm,qn}(t_1, t_2; \omega_1, \omega_2) = \frac{(\omega_{bw1} \omega_{bw2})^\eta}{(\omega_1 \omega_2)^{2\eta} (4\omega_1 \omega_2)} \Phi_\tau^{(-1)}(j(\omega_1 - \omega_2)) \Phi_T(j(\omega_2 - \omega_1)) \times \mathcal{W}(d_{p,q}^B, \mathcal{H}_{k_{1,2}}^B) \times \mathcal{W}(d_{m,n}^M, \mathcal{H}_{k_{1,2}}^M) \quad (3)$$

where $\Phi_T(\cdot)$ and $\Phi_\tau(\cdot)$ are the moment generating functions (MGF)s of clusters and path delays [4], $d_{(\cdot,\cdot)}^{(\cdot)} \triangleq [x, y, z, \cdot]^T$ is a separation vector indicating the antenna location, the time indices, the central frequencies and the MS direction and speed. $\mathcal{H}_{k_{1,2}} \triangleq \mathcal{G}_{p,k_{1,2}}(\omega_1) \otimes \mathcal{G}_{q,k_{1,2}}^*(\omega_2) \otimes (\mathcal{F}_{A,k_1} \mathcal{F}_{E,k_2})$ in which $\mathcal{G}_{(\cdot,\cdot,k_{1,2})}^{(\cdot)}(\omega)$, $\mathcal{F}_{A,k}$ and $\mathcal{F}_{E,k}$ are the k^{th} FSCs of the APP, the AAS and the EAS in corresponding antennas and/or coordinates [4]. $J_k(u)$ is the k^{th} -order Bessel function, \otimes represents the 2D linear convolution and $|\cdot|$ is the Euclidian norm. \mathcal{W} is defined as follows:

$$\mathcal{W}(d_{(\cdot,\cdot)}^{(\cdot)}, \mathcal{H}_{k_{1,2}}) \triangleq 2\pi \sum_{k_{1,2}=-\infty}^{+\infty} \left\{ \mathcal{H}_{k_{1,2}} j^{k_1} e^{j k_1 \arctan(\frac{x}{y})} \int_{-\frac{\pi}{2}}^{\frac{\pi}{2}} e^{j k_2 \Omega} e^{j \frac{z}{c} \sin \Omega} J_{k_1} \left(\cos \Omega \frac{\sqrt{x^2 + y^2}}{c} \right) d\Omega \right\} \quad (4)$$

III. NUMERICAL EVALUATION OF THE CCF

In this section, we numerically evaluate the derived CCF to see the impact of non-isotropic propagation, 3D APP and channel bandwidth.

A. Coherence Bandwidth of WB and UWB Channels

The CCF expression is used to determine the CB with the following equation: $CB = D_{\Delta\omega} = 0.5$, $D_{\Delta\omega} = \frac{|R(t_1, t_2; \omega_1, \omega_2)|^2}{|R(t_1, t_1; \omega_1, \omega_1)|^2}$ and $\Delta\omega = \omega_2 - \omega_1$. Figures 1 illustrates the CB depending on the channel delay spread (σ) and different values of the path-loss exponent. CB was determined for a bandwidth of 200MHz (2.4 ÷ 2.6MHz) and 7.5 GHz (3.1 ÷ 10.6GHz) for the WB and UWB channels, respectively. The results obtained for the CB are similar with the values obtained from experimental measurements [7], [8]. Although same delay spread were considered for both WB and UWB channels, lower CB values (higher frequency selectivity) were obtained for the UWB channel [8].

B. Fourier Analysis of the 3D-CCF for WB and UWB Channels in Stationary Scenario

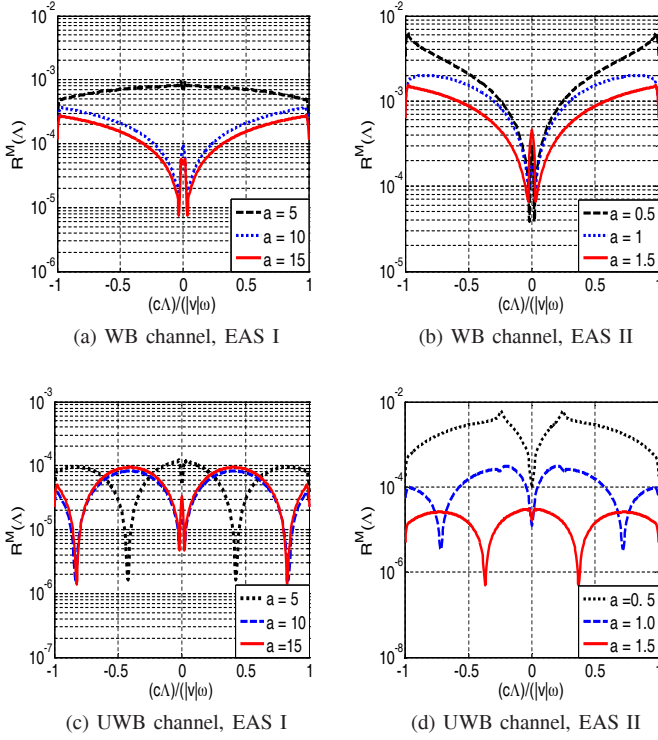


Fig. 2: 3D Power spectral density of WB (a, b) and UWB (c, d) channels, for EAS I , EAS II, AAS (Laplacian) non-isotropic pdfs and rectangular antenna.

We analyze the derived CCF in the frequency domain and in a simple multiple-input single-output (MISO) stationary scenario. The analysis is performed when $\omega_1, \omega_2 \triangleq \omega$; $m, n = 1$. In this case we obtain:

$$R_{1p,1q}(t_1, t_2, \omega, \omega) = 2\pi \frac{\omega_{bw}^{2\eta}}{\omega^{4\eta} 4\omega^2} \times \mathcal{W}(d_{p,q}^B, \mathcal{H}_{p,k_{1,2}}^M) \sum_{k_{1,2}=-\infty}^{\infty} \left\{ \mathcal{H}_{m,k_{1,2}}^M \times j^{k_1} e^{jk_1 \angle V} \int_{-\frac{\pi}{2}}^{\frac{\pi}{2}} e^{jk_2 \Omega} e^{j\frac{z}{c} \sin \Omega} J_{k_1} \left(\cos \Omega \frac{|V|}{c} \Delta t \right) d\Omega \right\} \quad (5)$$

Using (5) and Fourier transform of $J_{k_1}(u)$, the Fourier transform of the CCF versus Δt results in:

$$R^M(\Lambda) \triangleq \sum_{k_{1,2}=-\infty}^{\infty} \mathcal{H}_{1,k_{1,2}}^M e^{jk_1 \angle V} \int_{-\frac{\pi}{2}}^{\frac{\pi}{2}} \frac{e^{jk_2 \Omega} T_{k_1}(\Upsilon)}{\cos \Omega \sqrt{1 - \Upsilon^2}} d\Omega \quad (6)$$

Equation (6) represents the PSD for the 3D propagation environment, $R^M(\Lambda)$, where $\Upsilon = \frac{c\Lambda}{|V|\omega \cos \Omega}$. This expression illustrates the temporal variations of WB and UWB channels. As major concern of the current analysis is to see the effects of propagation in the third dimension (elevation), we assume Laplacian distribution for the AAS [4].

Figures 2 show the derived PSD for WB and UWB channels as a function of EAS I and EAS II with different values for a , with rectangular antenna and moving ($V=50\text{Km/h}$) on the positive x -axis direction. Results suggest that the PSD does not significantly depend on the urbanization factor a , but

changes with the EAS. It means that each EAS can be used to model a certain category of 3D non-isotropic propagation environments. At $\Lambda = 0$, PSD shows a peak which is the result of signal bandwidth, central frequency and Doppler shift; for the UWB channel, this peak is less pronounced due to increased signal dispersion caused by ultra-wide bandwidth of the APP and high central frequency [2], [5]. The PSD computed for the WB channel is pretty similar to what is presented for the NB channel presented in [2], with some differences due to WB/UWB characteristic. Comparing the PSDs obtained for NB (in [2]), WB and UWB channels, we conclude that the channel bandwidth has the major influence on the shape of the PSD.

IV. CONCLUSION

We have investigated the impact of 3D non-isotropic propagation along with channel bandwidth on the CCF of WB/UWB MIMO channels. The proposed model was developed based on closed-form formula that provides considerable insight into the relationship between characteristics of the propagation environment and the transmitted signal. Analysis of the CCF reveals the fact that the associated temporal PSD highly depends on the EAS and the channel bandwidth. On the other hand, CB depends on the channel bandwidth and the delay spread. To achieve uncorrelated MIMO channels, it is necessary to have small CB values which is much easier to achieve for UWB signals with bandwidth much larger than the channel CB. Results may be effectively employed in the fields like networking and signal processing where the channel time variations are important, e.g. signal detection, recognition, interception.

REFERENCES

- [1] A. F. Molisch, J. R. Foerster, and M. Pendergrass, "Channel models for ultra-wideband personal area networks," *IEEE Wireless Commun. Mag.*, vol. 10, no. 6, pp. 14–21, 2003.
- [2] H. S. Rad and S. Gazor, "Space-time-frequency characterization of 3D non-isotropic MIMO multicarrier propagation channels employing directional antennas," *EURASIP J. Wireless Commun. and Networking*, vol. 2008, 14 pages.
- [3] R. C. Qiu, "A study of the ultra-wideband wireless propagation channel and optimum UWB receiver design," *IEEE J. Sel. Areas Commun.*, vol. 20, no. 9, pp. 1628–1637, Dec. 2002.
- [4] A. M. Pištea, T. Palade, A. Moldovan, and H. S. Rad, "The impact of antenna directivity and channel bandwidth on the power spectral density of wideband and UWB MISO channels," in *Proc. ICWMC 2011*, pp. 36–41.
- [5] J. D. Parson and A. M. D. Turkmani, "Characterisation of mobile radio signals: base station crosscorrelation," *IEE Proc. I, Commun., Speech and Vision*, vol. 138, no. 6, pp. 557–565, Dec. 1991.
- [6] C. A. Balanis, *Antenna Theory: Analysis and Design*, 2nd edition. John Wiley & Sons, 1996.
- [7] M. O. Wessman, A. Svensson, and E. Agrell, "Frequency diversity performance of coded multiband-OFDM systems on IEEE UWB channels," *2004 IEEE Vehicular Technology Conference*.
- [8] G. Santella and E. Restuccia, "Analysis of frequency domain wide-band measurements of the indoor radio channel at 1, 5.5, 10, and 18GHz," in *Proc. 1996 Global Telecommunications Conference*, vol. 2, pp. 1162–1166.